Journal Name

ARTICLE TYPE

Cite this: DOI: 10.1039/xxxxxxxxxx

Linking slow dynamics and microscopic connectivity in dense suspensions of charged colloids†

Ruben Higler,[a] Johannes Krausser,[b] Jasper van der Gucht,[a] Alessio Zaccone,[b] and Joris Sprakel*[a]

Received Date
Accepted Date

DOI: 10.1039/xxxxxxxxxx

www.rsc.org/journalname

The quest to unravel the nature of the glass transition, where the viscosity of a liquid increases by many orders of magnitude, while its static structure remains largely unaffected, remains unresolved. While various structural and dynamical precursors to vitrification have been identified, a predictive and quantitative description of how subtle changes at the microscopic scale give rise to the steep growth in macroscopic viscosity is missing. It was recently proposed that the presence of long-lived bonded structures within the liquid may provide the long-sought connection between local structure and global dynamics. Here we directly observe and quantify the connectivity dynamics in liquids of charged colloids en-route to vitrification using three-dimensional confocal microscopy. We determine the dynamic structure from the real-space van Hove correlation function and from the particle trajectories, providing upper and lower bounds on connectivity dynamics. Based on these data, we extend Dyre's model for the glass transition to account for particle-level structural dynamics; this results in a microscopic expression for the slowing down of relaxations in the liquid that is in quantitative agreement with our experiments. These results indicate how vitrification may be understood as a dynamical connectivity transition with features that are strongly reminiscent of rigidity percolation scenarios.

1 Introduction

For fragile glasses, the super-exponential increase in viscosity with small changes in temperature is often described by the phenomenological Vogel-Fulcher-Tamman (VFT) relationship[1]. The VFT form holds for a wide variety of fragile glass formers, ranging from metallic[2,3] and molecular glasses[4,5] to those formed by polymer chains[6] or colloidal particles[7]. However, a microscopic interpretation of this universal observation remains elusive. Seminal frameworks for the glass transition, such as mode-coupling theory (MCT), accurately predict the mechanism with which particle motion becomes localised from the static structure alone[8], but cannot recover the VFT law for the viscosity or relaxation time. The case of charged particles interacting via long-ranged Coulombic potentials has been explored by MCT with a predicted vitrified phase as a result[9]. For several systems of charged colloids, a glassy phase, or Wigner glass, has been identified, including charged polystyrene particles[10] and highly charged clay platelets[11–17]. In all of these experiments, scattering methods have been used to probe the often complex ensemble-averaged sample dynamics. However, not much experimental data is available in these charged systems that resolve the structure and dynamics down to the single-particle level.

To understand and predict how structural relaxations slow down in colloidal suspension upon increasing the particle concentration, it has been suggested that the emergence of frequency-dependent rigidity must be taken into account. The presence of a finite shear modulus at low frequencies is predicted to underpin the slowing down of particle motion, and the concomittant increase in the apparent viscosity, also at finite temperature[18,19]. This finite-frequency rigidity cannot be understood solely from snapshots of the static structure. Rather, rigidity emerges from long-lived bonds between neighbouring particles[20,21], which are needed to suppress nonaffine motions characteristic of liquids. It was recently proposed that the same long-lived structures govern their thermodynamics such as their internal energy and specific heat[18]. This implies that long-lived bonded structures may play an important role in the liquid state. The hypothesized connection between such structures and the viscoelasticity of liquids has been verified indirectly, for example for metallic alloys and poly-

[a] Physical Chemistry and Soft Matter, Wageningen University & Research, Stippeneng 4, Wageningen, The Netherlands.
[b] Department of Chemical Engineering and Biotechnology, University of Cambridge, Cambridge CB3 0AS, United Kingdom.

† Electronic Supplementary Information (ESI) available: The Supplementary Information contains details on the particle synthesis and characterisation, sample preparation, determination of the pair potential and additional experimental data. See DOI: 10.1039/b000000x/

* Corresponding author; E-mail: joris.sprakel@wur.nl

mer melts[22,23]. Interestingly, within this picture due to the mobility and continuous restructuration of the liquid structure, rigidity emerges only beyond a finite and critical frequency. Within the approach of Frenkel, Trachenko and Brazhkin[18,24], this implies a continuous crossover from the liquid to the solid state, in which only the characteristic time-scale at which rigidity emerges becomes larger and larger; an idea recently proven experimentally[25]. While detailed studies of structure and dynamics in glassy liquids at the atomic or molecular scale are possible with a variety of scattering methods[26,27], which have revealed much of our current knowledge of glassy dynamics, these do not allow identification of bonds at the level of individual cages between single particles. This type of information is however accessible in colloidal suspensions visualized using confocal microscopy.

In colloidal liquids, where dynamical slowing down can be induced by changing the particle packing fraction, several microstructural and dynamical features have been identified to emerge as the liquid relaxations slow down and the glassy state is approached. While colloidal systems can by no means mimic all of the richness in phenomena found in atomic and molecular glasses, some crucial features can be observed and studied in colloidal systems as a proxy for these phenomena at much smaller scales. These range from the emergence of spatiotemporally heterogeneous dynamics[28–30] with features of criticality[31], localised "soft" vibrational modes[32] to structural signs in the form of icosahedral order[33], topological clusters[34,35] and persistent fractal structures that are proposed to percolate at the liquid-solid transition[36]. Nonetheless, a key question remains: Is there a direct and quantitative correlation between the microscopic dynamics of long-lived bonded structures and the slowing down of liquids en-route to kinetic arrest?

In this paper, we study suspensions of charged colloidal particles using three-dimensional confocal microscopy to identify and evaluate the dynamics of long-lived structures in colloidal liquids. We specifically chose colloids interacting through long-ranged electrostatic repulsions as this pushes the liquid-solid transition to lower volume fractions. This has the important advantage that surface interactions, such as frictional contacts and the resulting jamming, which may appear in colloidal hard-spheres, can be avoided possibly resulting in a cleaner view on the effects of local geometry on the suspension dynamics. In this approach, we have direct access to local structural dynamics at the single particle level. We directly obtain the dynamic coordination number in these experiments from real-space analysis. Based on these experiments, we reformulate Dyre's elastic model for liquid relaxations. To obtain a prediction for the global relaxation time, we use the dynamics of local coordination number as input to describe the finite-frequency shear modulus within the approach of marginal spring networks. This yields a theoretical model based on microscopic properties that is in agreement with the experimental data. These results indicate how structural bonding dynamics at the nearest-neighbor level govern the macroscopic viscosity of these liquids of charged colloids.

Methods

As an experimental model for charged colloids in apolar media, we use spherical particles, composed of poly(methyl methacrylate), stabilised by a comb-polymer of polyhydroxystearic acid grafts on a PMMA backbone at their surface. For details on the synthesis and characterization we refer to the SI. We use particles with radii $a_{small} = 710$ nm and $a_{large} = 975$ nm as determined by static light scattering, in a 1:1 ratio by volume. The particles are suspended in a density-matching mixture of *cis*-decalin and tetrachloroethylene containing 10 mM Aerosol OT as a charging agent[37]. Density matching conditions are established by adjusting the solvent mixture until we observe no visible sedimentation after centrifugation at 2000 g for 1 hour. This solvent mixture also has a similar refractive index to the particles, ensuring optical transparency and minimizing scattering, thus enabling observation deep into the sample with confocal microscopy. We load the suspension into glass sample chambers†(extended description of sample chamber construction in SI†), hermetically sealed using Norland Optical Adhesive. We image the samples using confocal fluorescence microscopy using a VT-Infinity3 confocal module from VisiTech International, mounted on a Nikon Ti-U inverted microscope. Images are captured with a Hamamatsu sCMOS ORCA-Flash4.0 camera. For most analysis we use three-dimensional image stacks recorded in time; we capture 2500 three-dimensional xyz-image stacks at 2 Hz, with a field of view of 205 x 205 x 75 voxels (voxel volume 0.25 x 0.25 x 0.33 μm^3). For the analysis of sample dynamics using the intermediate scattering function $F_s(\mathbf{q},t)$ we require a higher time resolution; to this end we record $30,000$ two-dimensional slices through our three-dimensional system at a frequency of 20 Hz. From the raw confocal images we extract the particle centroid positions with subpixel resolution using established algorithms both for two- and three-dimensional data[38], and link these together into particle trajectories. Recent advances in particle locating have lead to the development of locating algorithms which improve some weaknesses in the standard algorithms, in particular for suspensions in which the interparticle distance becomes comparable to the particle diameter, by means of iterative locating[39]. We have compared our data with results on the same data sets using these iterative algorithms and find no difference. Thus, in our case, the use of these enhanced algorithms does not lead to improvement in data. Due to the charges on the particle surface, the interparticle separation never approaches the particle diameter (Fig. S5 & S6†), such that the tracking accuracy is not enhanced by iterative routines. All other data analysis is performed using dedicated *MATLAB* scripts, which are available upon request from the authors.

Results

We study colloidal particles of poly(methyl methacrylate), stabilised by polyhydroxystearic acid, suspended in a density and refractive index matching mixture of apolar solvents†(see SI†for synthetic details). To suppress crystallization we use a binary mixture of particles with radii $a_{small} = 710$ nm and $a_{large} = 975$ nm as determined from light scattering. This gives a size ratio $a_{small}/a_{large} = 0.7$, which is known to effectively suppress crys-

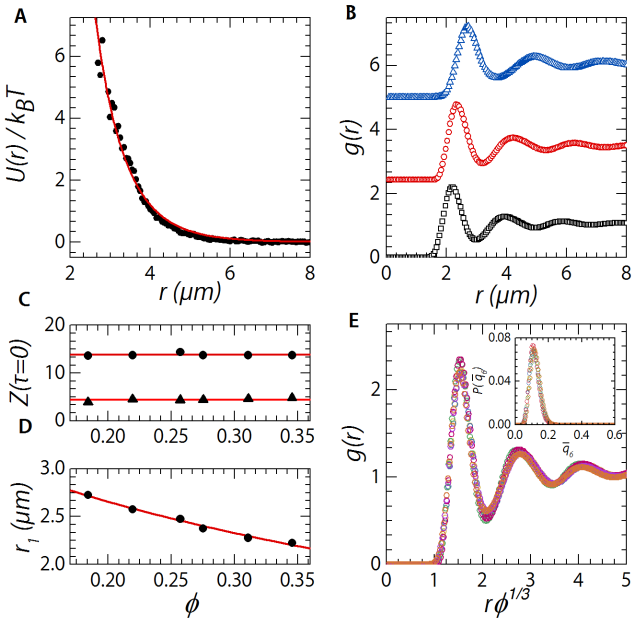

Fig. 1 (**A**) Pair interaction potential determined in the dilute limit ($\phi \approx 0.008$, symbols) and fitted to a Yukawa potential (line). (**B**) Pair correlation functions $g(r)$ for $\phi = 0.18$, 0.28 and 0.35 (top to bottom), horizontally offset for clarity. (**C**) Static coordination number $Z(\tau = 0)$ with a cut-off at the first neighbor distance r_1, taken as the first maximum in $g(r)$ (triangles), as r_2, the first minimum in $g(r)$ (circles). (**D**) Nearest-neighbor distance r_1 in $g(r)$ as a function of particle volume fraction (**E**) Pair correlation functions with a distance axis rescaled as $r\phi^{1/3}$, for ϕ =0.35, 0.31, 0.28, 0.26, 0.22, and 0.18. (**inset**) Probability distribution of the bond-orientational order parameter $\bar{q}_6$ showing a liquid structure and the absence of crystallites for ϕ =0.35, 0.31, 0.28, 0.26, 0.22, and 0.18.

tallisation[40]. The addition of 10 mM of the surfactant AOT leads to charging of the particles; in the apolar solvent this results in long-ranged repulsive interactions[37,41]. We image the particles in three dimensions and time using confocal fluorescence microscopy and determine their centre-of-mass positions with ~ 30 nm accuracy.

Inversion of the three-dimensional pair correlation function $g(r)$ can be used to gain insight into the particle interactions in the suspension. We use this approach in two different ways: i) in dilute suspensions and using an inversion based on the hypernetted-chain closure approximation to remove many-body effects can yield the two-body pair interaction potential[42?] , ii) in concentrated suspensions, simple inversion of the pair correlation function gives access to the potential-of-mean-force which probes the effective interactions between two particles in the presence of many others, which thus includes all many-body effects.

First, we start by determining the pair interactions by measuring the $g(r)$ of a dilute suspension at $\phi \approx 0.008$, and invert this using the hypernetted-chain closure approximation†(see SI†) to obtain the pair interaction potential (symbols in Fig. 1A). The experimental data are well-described by the Yukawa potential $U(r)/k_BT = \varepsilon \frac{\exp(-\kappa\sigma(\frac{r}{\sigma}-1))}{r/\sigma}$ (solid line in Fig. 1A) with $\sigma = 1.66$ μm , $1/\kappa = 1.0$ μm the Debye screening length and $\varepsilon/k_BT = 30.5$ the potential at contact.

At higher volume fractions ϕ, the instantaneous pair correlation function $g(r, \tau = 0)$, from a three-dimensional static snapshot of the sample, displays a liquid-like structure (Fig. 1B). As the volume fraction of particles is increased, the entire correlation function shifts monotonically to smaller values of r. This is shown by the shift in the position of the first peak r_1 as $r_1 \propto \phi^{-1/3}$, indicative of isotropic compression of the structure (Fig. 1D). Indeed, plotting the $g(r)$ for all volume fractions as a function of the rescaled parameter $r\phi^{1/3}$ places the positions of the structure peaks in the curve onto a single rescaled length scale (Fig. 1E), suggesting a almost homogeneous compression of the liquid structure, with little changes in its local geometry. This is corroborated by the fact that the instantaneous average coordination number $Z(\tau = 0)$ from snapshots of the liquid structure is virtually independent of ϕ (Fig. 1C); both when counting neighbors within a distance equal to the first maximum in $g(r)$ at r_1 and the first minimum in $g(r)$ at r_2. We note, as we will show below, that the shape of the peaks in $g(r)$, in particular the curvature of the peak at its maximum, are very weakly but systematically dependent on volume fraction, such that we cannot strictly speak of a full collapse of the $g(r)$ by rescaling the distance axis.

While we observe almost no changes in the local structure upon increasing the particle volume fraction, we find strong changes in particle dynamics across the same range of ϕ. We compute the intermediate scattering function $F_s(q,t)$ directly from our microscopy data as $F_s(q,t) = \langle \exp(i\mathbf{q}\cdot[\mathbf{r}(t) - \mathbf{r}(0)]) \rangle$ where we choose $q = 2\pi/r_1$ as the scattering vector. We find two distinct decays in the dynamic structure factors (Fig. 2A); at long lag times a structural α-relaxation is observed, which is typically associated with cage breaking and structural relaxations. At short times, the particles explore the confines of their geometric cages,

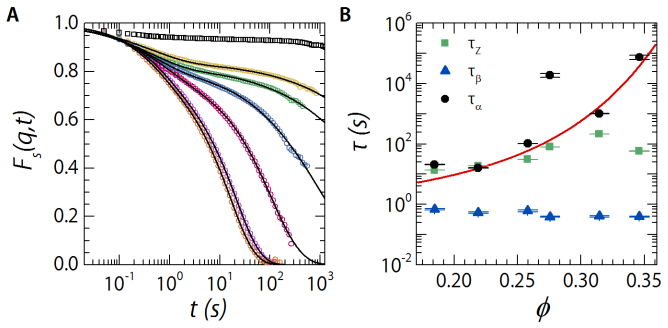

Fig. 2 (**A**) Self-intermediate scattering function $F_s(q,t)$ at $q = 2\pi/r_1$ for (top to bottom) $\phi = 0.49$, 0.35, 0.28, 0.31, 0.26, 0.22, and 0.18; solid lines are fits to a double stretched exponential decay as explained in the text. (**B**) Relaxation times for α- (black circles), β-relaxation processes (blue triangles), as extracted from $F_s(q,t)$, and as determined from the decay of the dynamical coordination number, $Z(\tau)$ (green squares). Solid line is description for τ_α, from the reformulated theory of Dyre. Error bars respresent the 95% confidence interval of the fit.

which results in a small β-decay at short times. These two processes are characterised by the relaxation times τ_α and τ_β, respectively; we extract these two characteristic time scales by fitting the experimental $F_s(q,t)$ to a double stretched exponential[7], $F_s(q,t) = A\exp\left[-(t/\tau_\beta)^\delta\right] + (1-A)\exp\left[-(t/\tau_\alpha)^\gamma\right]$, with stretch exponents $\sim 0.5-0.9$.

We note that due the inherent experimental constraints associated with particle-level imaging, the range of time scales that can be probed is limited. As a consequence, for the higher volume fractions the decay in $F_s(q,t)$ is only partially observed. We use these data nonetheless to extract a reasonable estimate for the structural relaxation time, but note that the accuracy of these values reduces as phi increases. Nonetheless, within experimental resolution we find a consistent trend in the growth of τ_α. For the highest volume fraction explored, we find no significant decay and hence this data set is not used for further analysis.

With increasing ϕ, the structural relaxation time grows as the liquid viscosity increases. At much larger volume fractions, $\phi > 0.40$, we see a time-independent plateau in $F_s(q,t)$ (black squares Fig. 2A), which indicates full dynamic arrest on experimental time scales. The β–relaxation time, extracted from $F_s(q,t)$ is virtually independent of ϕ and set by the in-cage particle diffusion coefficient, whereas the structural α–relaxation time grows steeply over more than 4 decades (Fig. 2B). Following previous experimental studies of colloidal glasses[7,43], we empirically identify the glass transition as the volume fraction where $\tau_\alpha/\tau_B = 10^5$, found at $\phi_g \approx 0.35$. We note that defining the exact point of vitrification along the different approaches that have been developed, such as mode-coupling theory[44], the random first-order transition approach[45] or the Adam-Gibbs theory[46], is not the focus of this paper. Hence we use the empirical criterion used more frequently in experimental studies of colloidal systems.

By fitting the measured pair potential in the dilute limit (Fig. 1A) we have determined that the Debye screening length under dilute conditions is $\kappa^{-1} = 1.0\mu$m. We can define an effective volume fraction, which takes the charge interactions into account, as $\phi_{\text{eff}} = \frac{4}{3}\pi(\bar{a}+\kappa^{-1})^3 n = (\bar{a}+\kappa^{-1})^3\phi/\bar{a}^3$, with n the number density of particles and $\bar{a}$ the geometric mean of particle radii, as we work in a bidisperse system at a 1:1 number ratio. At the glass transition $\phi_g = 0.35$, the effective volume fraction is predicted to be $\phi_{\text{eff}} = 0.77$, which is well above where either vitrification or jamming is expected to occur. This suggests that self-screening of the interactions may be relevant at these particle concentrations.

The Debye screening length of an electrolyte solution is given by $\kappa^{-1} = \sqrt{\frac{\varepsilon_r\varepsilon_0 k_B T}{2N_A e^2 I}}$[47], in which, ε_r and ε_0 are the dielectric constant of the solvent and the dielectric permittivity of vacuum, respectively, N_A is Avogadro's constant, e the elementary charge and I the ionic strength in the solution. In a medium with very low ionic strength, addition of charged colloids introduces additional counterions which contribute to screening of their own interactions. If we naively assume a homogeneous ion distribution, the overall ionic strength $I = I_b + I_c$ can be decomposed into that of the background solvent I_b and the contribution due to counterions of the particles I_c. We express the latter as a function of the colloid valency z, particle size R and volume fraction ϕ as $I_c = \frac{3\phi z}{4\pi\bar{a}^3(1-\phi)N_A}$.

For our experimental system, the screening length of the background solvent at very low colloid concentrations is $\kappa^{-1} = 1.0\mu$m. Knowing $\varepsilon_r = 2.5$, we deduce that the effective ionic strength of the background equals $I_b \approx 3$ μM. For the PMMA colloids we use, in presence of the charging agent AOT, previous experiments have shown that the particle valence z is low but can vary substantially between different batches. For the sake of argument, and to arrive at a qualitative understanding of the potential relevance of self-screening, we choose z =100 charges/particle, which was found to be a reasonable value for different batches by direct electrophoretic measurements[48]. At the glass transition $\phi_c \approx 0.35$, this naive approach predicts an increase in ionic strength due to counterions of $I_c \approx 40$ μM. As a consequence, the Debye screening length reduces to $\kappa^{-1} \approx 0.4$ μm, at which the effective colloid volume fraction becomes $\phi_{eff} = 0.52$, which is smaller than the glass transition predicted by MCT to occur at $\phi_g = 0.59$. The underestimation of the effective volume fraction is most likely due to ion correlations which will be significant in such underscreened systems. While an in-depth analysis would be required to detail these effects, this is not the purpose of this paper, but this naieve analysis at-least illustrates how non-trivial charge effects play a role. In our discussion we use the effective interactions from inversion of the pair correlation function to deal with these effects on a first-order phenomenological level.

The global dynamics could be influenced by local crystallinity or clustering of either particle species; as a check to make sure this is not the case we calculate the three dimensional bond-orientational order parameters, $\bar{q}_6$, for our system using the approach of Lechner et al.[49]. These data show a complete absence of any local crystalline structure, as indicated by the single peak around $\bar{q}_6 = 0.1$. (Fig. 1E inset)[49]. We are furthermore unable to find any ordered clusters of significant size for either particle species (Fig. S3†).

We observe virtually no changes in the static coordination number, from snapshots of the liquid structure, as a function of parti-

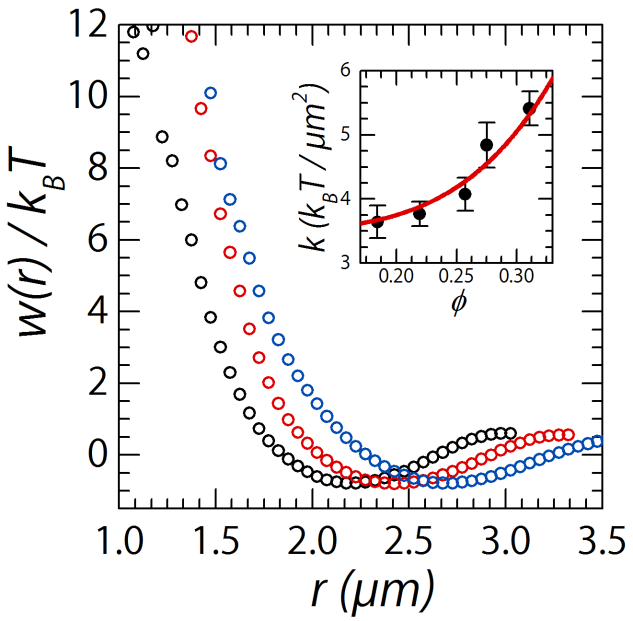

Fig. 3 The potential of mean force $w(r)$, determined from inversion of the $g(r)$ at finite volume fractions $\phi = 0.31$, 0.26, and 0.18. **Inset** Effective spring constant k of the particle-particle bonds, as determined from the curvature of $w(r)$.

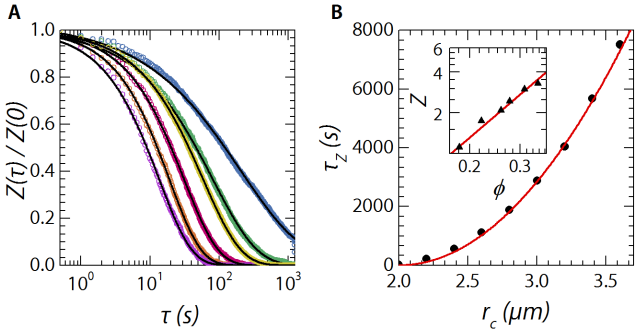

Fig. 4 (**A**) Decay of the normalised coordination number $Z(t)/Z(0)$ as calculated from experimental particle trajectories, for different volume fractions (left to right) $\phi = 0.18$, 0.22, 0.26, 0.35, 0.28, and 0.31. We set the neighbour cutoff distance r_c to the first minimum of $g(r)$, such that we only take the particle inside the first coordination shell into account. Solid lines are stretched exponential fits for the determination of τ_Z. (**B**) Typical decay time of $Z(\tau)/Z(0)$ as a function of neighbour cutoff distance r_c. Calculated from experimental trajectory data for $\phi = 0.31$. Solid red line is a power law fit with an exponent of two. (**inset**) Average coordination number Z at the Brownian timescale τ_B as a function of volume fraction. Calculated from the particle tracks (triangles) and Van Hove functions (circles). Solid lines are power law fits to the data.

cle volume fraction, from the dilute liquid state to the kinetically arrested state at $\phi > \phi_g$. Over the same range of volume fractions, the particle diffusivity slows down by many orders-of-magnitude. This is a characteristic feature of the glass transition and highlights, as is the main challenge in understanding how the dynamical slowing down in liquids occurs, that the arrest of relaxations in the liquid cannot be explained from the static structure alone. It was recently proposed that the slowing down of relaxation processes in liquids upon decreasing temperature, or increasing density, may be understood by considering how visco-elasticity emerges at finite frequency due to the formation of persistent bonds between neighboring particles[18,22,23]. This approach thus does not rely on the static structure, but rather takes the transient nature of neighboring particle pairs into account, to evaluate their significance in contributing to the actual local rigidity of the structure.

This concept assumes that particles are capable of forming cohesive bonds. By contrast, our experimental system is composed of particles interacting with a purely repulsive pair potential (Fig. 1A), hence cohesion must be an emergent property caused by many-body correlations. These bonds can be defined as the presence of two particles in a close-enough proximity which enables them to carry a mechanical load, and thus contribute to the rigidity of the material. Despite the lack of cohesive forces, colloidal suspensions can develop a shear modulus[47] even when the interactions are purely repulsive, due to the formation of these effective 'bonds', or contacts which can carry a shear stress, when the suspension is contained at a finite fixed pressure.

Inversion of the pair-correlation function at finite volume fractions allows us to directly measure the potential-of-mean-force $w(r) = -\ln g(r)$ between the particles. These exhibit a clear bonding minimum at a distance that corresponds to the characteristic nearest-neighbor distance r_1. This illustrates how, even in purely repulsive systems at a finite pressure, effective bonds emerge as a many-body effect.

These same emergent bonds allow repulsive colloidal systems to build up a finite elastic shear modulus, as demonstrated extensively in the literature[47]. The spring constant k that characterises the stiffness of these bonds, obtained by fitting the minimum in $w(r)$ to a harmonic well, increases slightly with increasing volume fraction; its absolute value of k =3.5-5.5 $k_BT/\mu m^2$ is of order k_BT/r_1^2 as expected for a system governed by soft interactions (Fig. 3). We note that while the rescaling of $g(r)$ with $r\phi^{1/3}$ yields a collapse of the *position* of the curve, the width of the peaks narrows by a small amount as the volume fraction is increased, signifying a slight increase in the bond stiffness as expressed by the increase in k with ϕ.

To ascertain the dynamics of these bonds that emerge in liquids of repulsive particles, we aim to extract the dynamical coordination number $Z(\tau)$ from our three-dimensional confocal microscopy data. This quantity probes how an initial set of nearest-neighbours exchanges as time progresses; while the average coordination number at any given snapshot may remain the same, particle motion will reshape the cages around a reference particle by breaking existing bonds and reforming new ones such that $Z(\tau)/Z(0) < 1$. We note that other metrics for probing the restructuring of confining cages exist, e.g. that proposed by Rabani et al.[50–52]; here we choose specifically to use $Z(t)$ which can be obtained directly from our particle-level experimental data without any arbitrary parameter choices and has been used successfully in the past to probe nearest-neighbor bond relaxation[36,53,54] and is thus established as a reliable metric.

We can determine $Z(\tau)$ directly from the three-dimensional par-

ticle trajectories, as was previously done for hard-sphere suspensions and attractive colloidal systems[21,36,54]. For every particle, at a given reference time, we identify its neighbors within a cut-off distance r_c, which we set equal to the first minimum in $g(r)$, at a lag time of $\tau = 0$ to find $Z(0)$. We then compute the time-trace of the separation distance between a probe particle, i, and its neighbours, j, as a fuction of lag times, $d_{ij}(\tau) = |\mathbf{r}_i(\tau) - \mathbf{r}_j(\tau)|$. A neighbor exchange, and thus a loss of the original configuration of neighbors, is identified when $d \leq r_c$, for a given pair, allowing us to construct $Z(\tau)$. To ensure sufficient statistics we perform time- and ensemble averaging, yielding $Z(\tau)$ as shown in Figure 4A.

To test the effect of the length scale r_c on the erosion of a given bonding configuration, we determine the decay time τ_Z of $Z(\tau)/Z(0)$, by fitting $Z(\tau)/Z(0)$ with a stretched exponential, as a function of r_c, for $\phi = 0.31$ (symbols in Fig. 4B). We find $\tau_Z \propto r_c^2$ (solid line Fig. 4B), indicating the diffusive nature of neighbour exchange processes. The stretched exponential nature of these connectivity relaxations is related to the stretched exponential decay of self-relaxations as probed by the self-intermediate scattering function and hints at heterogeneous dynamics, well established to emerge in colloidal system upon approaching their glass transition point[28,29].

We emphasize that the nearest-neighbor exchange dynamics probed by $Z(\tau)$ is a different measure for relaxations in the liquid than the self-mobility probed in $F_s(q,t)$, but rather is a collective (or distinct) effect. The dynamical coordination number probes how particles move with respect to its bonded neighbors. For example, the sliding of two particles with respect to each other, while remaining bonded, or the collective plug-like motion of a cluster of particles in a shear-transformation zone, does not lead to a reduction in Z but does lead to a decorrelation of $F_s(q,t)$. By contrast, cage rattling may break bonds such that $Z(\tau)$ decays while it results in only very weak decay in the dynamic structure factor. Indeed, the characteristic timescale for reconfiguration of a coordination shell τ_Z is lower and grows less steeply than τ_α obtained from fitting $F_s(q,t)$ (Fig. 2B).

Of special interest is the change in of $Z(\tau)$ as a function of ϕ as this provides a clue to the effect of local coordination dynamics on the volume fraction induced quenching of relaxation processes. At high frequencies, i.e. short τ, the scaling of Z with ϕ is weak, as both dilute and denser liquids have most of their original neighbors still in place (Fig. 4A). The differences between fast and slowly relaxing liquids become increasingly pronounced as the frequency is reduced, and concomitantly the steepness with which Z grows with ϕ increases.

So far we considered only the ensemble-average coordination number; however, a prototypical feature of liquids that slow down and approach their glass transition is that their dynamics become strongly heterogeneous[28–30]. To probe the spatial homogeneity of coordination structures, we reconstruct our experimental data by colour-coding particles according to their dynamical coordination number Z, taken both as the static structure $Z(\tau = 0)$, at the Brownian timescale $Z(t = \tau_B \sim 10^1 s)$, and at long timescales $Z(\tau = 250\ s)$. Indeed, we observe not only how the average coordination number at the Brownian timescale, $Z(t = \tau_B)$, decreases as the volume fraction is reduced (Fig. 6 middle row), but also how the distribution of coordination numbers is strongly heterogeneous in space (Fig. 5). From the reconstructions it is also clear that the debonding events through which the sample loses rigidity do not occur homogeneously throughout the sample; areas of high connectivity stay connected while areas with low connectivity weaken rapidly. Due to the heterogeneity of local coordination numbers, as observed in the reconstructed experimental data, the distribution of static coordination numbers $P(Z)$ for $\tau = 0$ is broad. However on average it is constant as a function of volume fraction (top row in Fig. 6). As lag time increases and the liquid relaxes, $P(Z(\tau = \tau_B))$ shifts to lower values and narrows with volume fraction (middle row in Fig. 6). At long lag times, most of the original neighbours have translated away and the liquid has fully relaxed (bottom row in Fig. 6).

Discussion & Conclusion

We observe a marked increase in structural relaxation time over 4 orders-of-magnitude upon increasing ϕ during which the static coordination number $Z(0)$ remains virtually constant. This is a well-established feature of most glassy systems and implies that relaxation slowdown cannot be understood from considering static structures alone. It was recently proposed that, rather than using the static structure as a starting point to explain the dynamical slow down, one should consider those bonds which are sufficiently long-lived to contribute to rigidity at relevant frequencies[22], in other words, it is suggested that we need to consider the structural dynamics of those neighbors that share load-bearing bonds.

In order for local structure to contribute to rigidity, the cage that surrounds a central particle, needs to be intact for a least as long as the required time of escape. Bonds that break before the attempted escape from a cage, do not contribute to the slowing down of particle dynamics. The characteristic timescale of particle escape from a cage will be of the order of the Brownian time scale $\tau_B = a^2/D \sim 10^1$ s, with D the particle self-diffusion coefficient. Thus, bonds which live longer than τ_B can contribute to a stable interconnected structure that provides the liquid with shear rigidity at Brownian frequencies. The concept that long-lived neighbors contribute to the formation of rigid structure in the liquid, revolves around the idea that the transition from a liquid-like to a solid-like response is signalled by the formation of an isostatic structure of load-bearing bonds at a characteristic frequency. Note that this is not the same as the zero-frequency liquid-solid transition, which is the focus of the jamming framework and which signals the arrest of flow on all timescales. Rather, the location of this frequency-dependent liquid-solid transition in these thermal fluids will depend on the choice of frequency[25]; for the purposes of this discussion we use the characteristic frequency $\omega_B = 1/\tau_B$.

From the experimental data for $Z(\tau)$, we can measure the value of the coordination number at $\tau = \tau_B$ as a proxy for the amount of bonds that could contribute to rigidity (inset Fig. 4B). We find that $Z(\tau_B)$ grows as the particle volume fraction is increased, whereas the static coordination number $Z(\tau = 0)$ remains constant over the same range of volume fractions (Fig. 1C).

For the frequency of interest, ω_B, a liquid-solid transition must

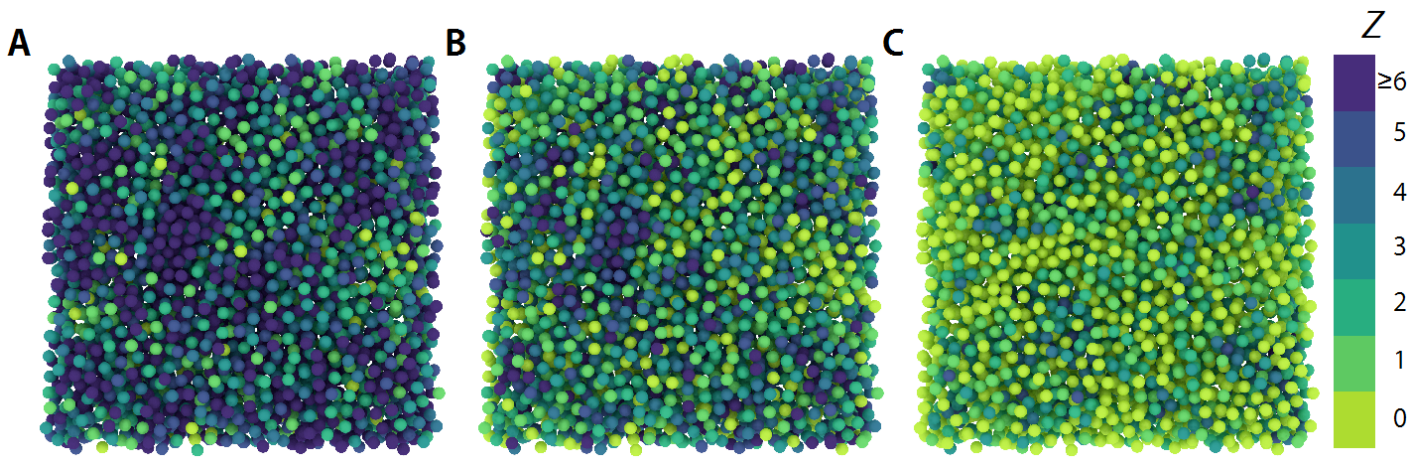

Fig. 5 Computer-generated renderings of our experimental system, in which the particles are color-coded according to their actual coordination number.(**A**): $Z(\tau = 0)$, (**B**): $Z(\tau = \tau_B)$, and (**C**): $Z(\tau = 250\ s)$. Dark blue particles have $Z \geq Z_c$, while particles with $Z < 6$ are colored in increasing shades of yellow, shown for $\phi = 0.31$.

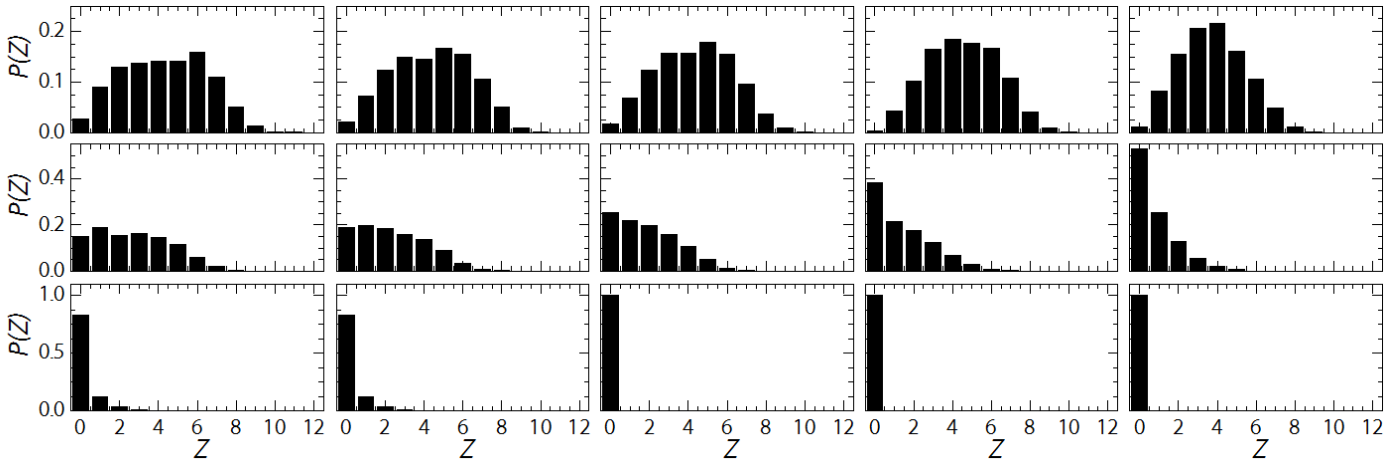

Fig. 6 Probability distribution of coordination numbers. For (left to right) $\phi = 0.31$, 0.28, 0.26, 0.22, and 0.18 we show the probability distribution of coordination numbers $P(Z)$. **top row,** Probability distributions of $Z(\tau = 0)$, the static coordination number. **middle row** Probability distributions of $Z(\tau = \tau_B)$. **bottom row** Probability distributions of $Z(\tau = 250\ s)$.

emerge at some critical volume fraction ϕ_c, where in accord with the Maxwell criterion for isostaticity in three-dimensional central-force lattices, $Z(\tau_B) = Z_c = 6$. To link the emergence of frequency-dependent elasticity to the slowing down of particle dynamics, we adopt the phenomenological model developed by Dyre. This approach treats relaxation events, occurring at finite frequency, as localized shear deformations of the surrounding medium; such local shear transformations have been observed experimentally in dense colloidal suspensions[55]. By combining thermally-activated dynamics of the Eyring type with continuum mechanics, Dyre analytically derived a relationship between the structural relaxation time and the shear modulus G of the liquid[56] as $\tau_\alpha = \tau_B \exp\left[\frac{GV_a}{k_BT}\right]$, where V_a is the activation volume. The term $E_a = GV_a$ represents the elastic activation energy to expand the cage allowing an irreversible rearrangement to take place. It is important to note that in Dyre's model, the local shear rigidity is described by the high-frequency shear modulus, which is close to predictions from affine elasticity.

A microscopic interpretation of the shear modulus is provided by the framework for disordered bead-spring lattices[57], which gives the affine shear modulus as[20]; $G = \frac{1}{5\pi}\frac{k(\phi)}{r_1(\phi)}\phi Z$, with k the effective spring constant of the interparticle bonds, which depends on ϕ (inset Fig. 3) and r_1 the average interparticle spacing. We note that this formulation unites the models of Dyre and Frenkel[24,56], where the term GV_a is the density of elastic potential energy, since the spring constant is the curvature of the minimum in the potential of mean force, multiplied by the number of connections Z, divided by r_1 gives us the total potential energy density experienced by a particle within a parabolic approximation.

As discussed above, even though we work with repulsive colloidal particles, effective bonds emerge as a many-body phenomenon (Fig. 3) whose spring constant $k(\phi)$ grows and average interparticle distance r_1 shrinks slightly as ϕ increases (inset Fig. 3 & Fig. 1D).

We estimate the activation volume V_a as the cage volume $V_a = \frac{4}{3}\pi r_1(\phi)^3$. We now obtain a version of Dyre's elastic model in terms of particle-level quantities:

$$\tau_\alpha = \tau_B \exp\left[\frac{4k(\phi)r_1(\phi)^2 Z(\phi)\phi}{15k_BT}\right] \quad (1)$$

in which the microscopic parameters can be directly extracted from the experiments. To evaluate the local connectivity Z, we must realise that rigidity in the liquid state only emerges above a finite frequency[18,24]; this raises the question what the appropriate frequency is to evaluate Z. Within the picture of Frenkel[24], the characteristic frequency at which rigidity should be evaluated corresponds to the attempt frequency of particle escape from their cage. In our case, the characteristic attempt frequency $\omega_0 \propto 1/\tau_B$, such that we must take $Z(\tau_B)$ as the appropriate measure for local connectivity (inset Fig. 4B). If we presume that the dependence of $Z(\tau_B)$ with volume fraction obeys a scaling, $Z(\tau_B) = Z_c(\frac{\phi}{\phi_c})^b$, we can identify a solid-liquid transition point at ϕ_c. However, our experimental data does not span a large enough range of volume fractions to draw a rigorous conclusion if this power-law scaling is found. Thus, we assume it to hold, and find by comparing the limited amount of experimental data to this form, $b = 1.8$ and $\phi_c \sim 0.45$ (inset Fig. 4B). A true test of the validity of this rigidity collapse argument requires an in-depth study of the local structure with volume fraction e.g. by means of extensive computer simulations, which is beyond the scope of this paper. This allows us to reformulate the equation in terms of directly observable quantities alone:

$$\tau_\alpha = \tau_B \exp\left[\frac{4k(\phi)r_1(\phi)^2 Z_c \phi^{1+b}\phi_c^{-b}}{15k_BT}\right] \quad (2)$$

This model provides a reasonable agreement with experimentally determined values for the relaxation time τ_α (solid line in Fig. 2B). We note that this is a model based only on directly observable microstructural properties, which gives a predictive connection between the liquid structure and the emergence of rigidity at finite frequency. Thus, this form reconciles the approaches of Dyre and Frenkel[24,56].

The agreement between experimental data and this theory illustrates how liquid viscosity at the global scale could possibly be understood from the existence and dynamics of long-lived, or persistent, emerging bonds between neighbouring particles. This may also imply that the slowing down of liquid relaxation processes, in analogy to those in metallic alloy melts or polymer fluids[22,23], is a dynamical connectivity transition leading to the isostatic condition at a finite, relevant, frequency. This conclusion is in direct agreement with the conceptual picture of fluidity and rigidity first proposed by Frenkel[24], and expanded on by Trachenko and Brazhkin[18], in which vitrification is a continuous transition in which the characteristic frequency at which rigidity emerges shrinks as the solid state is approached. The emergence of rigidity in liquids far away from any macroscopic phase transition was recently evidenced also for molecular systems, further supporting our claims[25]. A more complete understanding of the link between connectivity and the slowing down of relaxation processes, and its relation to the glass transition, requires a more detailed theoretical analysis of the problem, in which the frequency-dependence is treated explicitly and the spatial inhomogeneity and heterogeneous dynamics are taken into account[58].

Conflict of interest

There are no conflicts to declare.

Acknowledgements

The authors thank Ties van de Laar, Remco Fokkink and Raoul Frijns for technical assistance with particle synthesis and characterisation.

References

1 C. A. Angell, *Journal of non-crystalline solids*, 1988, **102**, 205–221.
2 A. L. Greer, *Science*, 1995, **267**, 1947–1953.
3 H. Wagner, D. Bedorf, S. Küchemann, M. Schwabe, B. Zhang, W. Arnold and K. Samwer, *Nature materials*, 2011, **10**, 439–442.

4 L. M. Martinez and C. A. Angell, *Nature*, 2001, **410**, 663–667.
5 C. A. Angell, *Science*, 1995, **267**, 1924–1935.
6 D. Huang, D. M. Colucci and G. B. McKenna, *The Journal of Chemical Physics*, 2002, **116**, 3925–3934.
7 G. Brambilla, D. El Masri, M. Pierno, L. Berthier, L. Cipelletti, G. Petekidis and A. B. Schofield, *Physical Review Letters*, 2009, **102**, 085703.
8 W. Götze, *Complex Dynamics of Glass-Forming Liquids*, OUP Oxford, 2012.
9 S. K. Lai and S. Y. Chang, *Phys. Rev. B*, 1995, **51**, 12869–12872.
10 T. Palberg, E. Bartsch, R. Beyer, M. Hofmann, N. Lorenz, J. Marquis, R. Niu and T. Okubo, *Journal of Statistical Mechanics: Theory and Experiment*, 2016, **2016**, 074007.
11 B. Abou, D. Bonn and J. Meunier, *Phys. Rev. E*, 2001, **64**, 021510.
12 D. Bonn, H. Tanaka, G. Wegdam, H. Kellay and J. Meunier, *EPL (Europhysics Letters)*, 1999, **45**, 52.
13 B. Ruzicka, L. Zulian and G. Ruocco, *Journal of Physics: Condensed Matter*, 2004, **16**, S4993.
14 B. Ruzicka, L. Zulian and G. Ruocco, *Phys. Rev. Lett.*, 2004, **93**, 258301.
15 R. Bandyopadhyay, D. Liang, H. Yardimci, D. A. Sessoms, M. A. Borthwick, S. G. J. Mochrie, J. L. Harden and R. L. Leheny, *Phys. Rev. Lett.*, 2004, **93**, 228302.
16 A. S. Negi and C. O. Osuji, *Phys. Rev. E*, 2010, **82**, 031404.
17 D. Saha, Y. M. Joshi and R. Bandyopadhyay, *Soft Matter*, 2014, **10**, 3292–3300.
18 K. Trachenko and V. V. Brazhkin, *Scientific reports*, 2013, **3**, 2188.
19 Z. Zhang, N. Xu, D. T. N. Chen, P. Yunker, A. M. Alsayed, K. B. Aptowicz, P. Habdas, A. J. Liu, S. R. Nagel and A. G. Yodh, *Nature*, 2009, **459**, 230–233.
20 A. Zaccone and E. Scossa-Romano, *Physical Review B*, 2011, **83**, 184205.
21 M. Laurati, P. Maßhoff, K. J. Mutch, S. U. Egelhaaf and A. Zaccone, *Phys. Rev. Lett.*, 2017, **118**, 018002.
22 J. Krausser, K. H. Samwer and A. Zaccone, *Proceedings of the National Academy of Sciences*, 2015, **112**, 13762–13767.
23 A. Lappala-Vernon, A. Zaccone and E. Terentjev, *Soft Matter*, 2016, 7330–7337.
24 J. Frenkel, *Trans. Faraday Soc.*, 1937, **33**, 58–65.
25 L. Noirez and P. Baroni, *Journal of Physics: Condensed Matter*, 2012, **24**, 372101.
26 H. W. Sheng, W. K. Luo, F. M. Alamgir, J. M. Bai and E. Ma, *Nature*, 2006, **439**, 419 EP –.
27 Y. H. Liu, G. Wang, R. J. Wang, D. Q. Zhao, M. X. Pan and W. H. Wang, *Science*, 2007, **315**, 1385–1388.
28 E. R. Weeks, J. C. Crocker, A. C. Levitt, A. Schofield and D. A. Weitz, *Science*, 2000, **287**, 627–631.
29 L. Berthier, G. Biroli, J.-P. Bouchaud, L. Cipelletti and W. van Saarloos, *Dynamical Heterogeneities in Glasses, Colloids, and Granular Media*, Oxford University Press, 2011.
30 L. O. Hedges, R. L. Jack, J. P. Garrahan and D. Chandler, *Science*, 2009, **323**, 1309–1313.
31 H. Tanaka, T. Kawasaki, H. Shintani and K. Watanabe, *Nature materials*, 2010, **9**, 324–331.
32 K. Chen, M. L. Manning, P. J. Yunker, W. G. Ellenbroek, Z. Zhang, A. J. Liu and A. G. Yodh, *Physical Review Letters*, 2011, **107**, 108301.
33 M. Leocmach and H. Tanaka, *Nature communications*, 2012, **3**, 974.
34 A. Malins, J. Eggers, C. P. Royall, S. R. Williams and H. Tanaka, *The Journal of Chemical Physics*, 2013, **138**, 12A535.
35 C. P. Royall, S. R. Williams, T. Ohtsuka and H. Tanaka, *Nature materials*, 2008, **7**, 556–561.
36 J. C. Conrad, P. P. Dhillon, E. R. Weeks, D. R. Reichman and D. A. Weitz, *Physical Review Letters*, 2006, **97**, 265701.
37 T. Kanai, N. Boon, P. J. L. éŹÿè£ŕç¿ľ, E. Sloutskin, A. B. Schofield, F. Smallenburg, R. van Roij, M. Dijkstra and D. A. Weitz, *Physical Review E*, 2015, **91**, 030301.
38 Y. Gao and M. L. Kilfoi, *Optics express*, 2009, **17**, 4685–4704.
39 K. E. Jensen and N. Nakamura, *Review of Scientific Instruments*, 2016, **87**, 066103.
40 D. B. Miracle, D. V. Louzguine-Luzgin, L. V. Louzguina-Luzgina and A. Inoue, *International Materials Reviews*, 2013, **55**, 218–256.
41 A. Yethiraj and A. van Blaaderen, *Nature*, 2003, **421**, 513–517.
42 S. H. Behrens and D. G. Grier, *Physical Review E*, 2001, **64**, 050401.
43 J. Mattsson, H. M. Wyss, A. Fernandez-Nieves, K. Miyazaki, Z. Hu, D. R. Reichman and D. A. Weitz, *Nature*, 2009, **462**, 83–86.
44 W. van Megen and S. M. Underwood, *Phys. Rev. E*, 1994, **49**, 4206–4220.
45 G. Biroli and J.-P. Bouchaud, in *The Random First-Order Transition Theory of Glasses: A Critical Assessment*, John Wiley & Sons, Inc., 2012, pp. 31–113.
46 G. Adam and J. H. Gibbs, *The Journal of Chemical Physics*, 1965, **43**, 139–146.
47 W. B. Russel, D. A. Saville and W. R. Schowalter, *Colloidal Dispersions*, Cambridge University Press, 1989.
48 S. K. Sainis, J. W. Merrill and E. R. Dufresne, *Langmuir*, 2008, **24**, 13334–13337.
49 W. Lechner and C. Dellago, *The Journal of Chemical Physics*, 2008, **129**, 114707.
50 E. Rabani, J. D. Gezelter and B. J. Berne, *The Journal of Chemical Physics*, 1997, **107**, 6867–6876.
51 E. Rabani, J. D. Gezelter and B. J. Berne, *Phys. Rev. Lett.*, 1999, **82**, 3649–3652.
52 J. D. Gezelter, E. Rabani and B. J. Berne, *The Journal of Chemical Physics*, 1999, **110**, 3444–3452.
53 D. Heckendorf, K. J. Mutch, S. U. Egelhaaf and M. Laurati, *Phys. Rev. Lett.*, 2017, **119**, 048003.
54 Z. Zhang, P. J. Yunker, P. Habdas and A. Yodh, *Physical review*

letters, 2011, **107**, 208303.
55 P. Schall, D. A. Weitz and F. Spaepen, *Science*, 2007, **318**, 1895–1899.
56 J. C. Dyre, *Journal of non-crystalline solids*, 1998, **235-237**, 142–149.
57 A. Zaccone and E. M. Terentjev, *Physical Review Letters*, 2013, **110**, 178002.
58 J. P. Garrahan and D. Chandler, *Physical Review Letters*, 2002, **89**, 035704.